Arctiin attenuates iron overload-induced osteoporosis by regulating the PI3K/Akt pathway

MIAO LI[1,2*], ZHAOFENG PAN[1,2*], QI HE[1,2*], JIACONG XIAO[1,2], BAIHAO CHEN[1,2], FANCHEN WANG[1,2], PAN KANG[1,2], HAORAN LUO[1,2], JIANLIANG LI[1,2], JIAXU ZENG[1,2], SHAOCONG LI[1,2], JUNZHENG YANG[1,2], HAIBIN WANG[1-3] and CHI ZHOU[1-4]

[1]First School of Clinical Medicine, [2]The Laboratory of Orthopedics and Traumatology of Lingnan Medical Research Center, Guangzhou University of Chinese Medicine; [3]Department of Orthopedic Surgery, The First Affiliated Hospital, Guangzhou University of Chinese Medicine, Guangzhou, Guangdong 510405; [4]Maoming Hospital of Guangzhou University of Chinese Medicine, Maoming, Guangdong 525022, P.R. China

Received July 4, 2023; Accepted September 7, 2023

DOI: 10.3892/ijmm.2023.5311

Abstract. Iron overload is a prevalent pathological factor observed among elderly individuals and those with specific hematological disorders, and is frequently associated with an elevated incidence of osteoporosis. Although arctiin (ARC) has been shown to possess antioxidant properties and the ability to mitigate bone degeneration, its mechanism of action in the treatment of iron overload-induced osteoporosis (IOOP) remains incompletely understood. To explore the potential molecular mechanisms underlying the effects of ARC, the MC3T3-E1 cell osteoblast cell line was used. Cell Counting Kit was used to assess MC3T3-E1 cell viability. Alkaline phosphatase staining and alizarin red staining were assessed for osteogenic differentiation. Calcein AM assay was used to assess intracellular iron concentration. In addition, intracellular levels of reactive oxygen species (ROS), lipid peroxides, mitochondrial ROS, apoptosis rate and mitochondrial membrane potential changes in MC3T3-E1 cells were examined using flow cytometry and corresponding fluorescent dyes. The relationship between ARC and the PI3K/Akt pathway was then explored by western blotting and immunofluorescence. In addition, the effects of ARC on IOOP was verified using an iron overload mouse model. Immunohistochemistry was performed to evaluate expression of osteogenesis-related proteins. Micro-CT and H&E were used to analyze bone microstructural parameters and histomorphometric indices in the bone tissue. Notably, ARC treatment reversed the decreased viability and increased apoptosis in MC3T3-E1 cells originally induced by ferric ammonium citrate, whilst promoting the formation of mineralized bone nodules in MC3T3-E1 cells. Furthermore, iron overload induced a decrease in the mitochondrial membrane potential, augmented lipid peroxidation and increased the accumulation of ROS in MC3T3-E1 cells. ARC not only positively regulated the anti-apoptotic and osteogenic capabilities of these cells via modulation of the PI3K/Akt pathway, but also exhibited antioxidant properties by reducing oxidative stress. *In vivo* experiments confirmed that ARC improved bone microarchitecture and biochemical parameters in a mouse model of iron overload. In conclusion, ARC exhibits potential as a therapeutic agent for IOOP by modulating the PI3K/Akt pathway, and via its anti-apoptotic, antioxidant and osteogenic properties.

Correspondence to: Professor Chi Zhou or Professor Haibin Wang, Department of Orthopedic Surgery, The First Affiliated Hospital, Guangzhou University of Chinese Medicine, 16 Jichang Road, Baiyun, Guangzhou, Guangdong 510405, P.R. China
E-mail: zcmzy1@163.com
E-mail: hipman@163.com

*Contributed equally

Abbreviations: ALP, alkaline phosphatase; ARC, arctiin; ARS, Alizarin Red S; BV/TV, bone volume/tissue volume; Col I, collagen type I; FAC, ferric ammonium citrate; IOOP, iron overload-induced osteoporosis; LPO, lipid peroxidation; MMP, mitochondrial membrane potential; mtROS, mitochondrial reactive oxygen species; Runx2, Runt-related transcription factor 2; SMI, structure model index; Tb.N, trabecular bone number; Tb.Pf, trabecular bone pattern factor; Tb.Sp, trabecular separation/spacing; Tb.Th, trabecular thickness; micro-CT, micro-computed tomography

Key words: arctiin, iron overload, osteoporosis, PI3K/Akt, reactive oxygen species

Introduction

Osteoporosis is a prevalent age-related chronic condition characterized by a decrease in bone mass and disrupted alignment of bone trabeculae, which has been reported to be influenced by iron levels in the body (1,2). Consequently, it has been hypothesized that age-associated iron overload and oxidative stress serve pivotal roles in the development of osteoporosis.

Iron serves an important role in a wide range of physiological functions, including oxygen transport, enzyme reactions, energy production, protein synthesis and DNA repair (3). Iron metabolism is rigorously regulated by numerous factors and when this equilibrium is disrupted, iron overload leads

to elevated levels of reactive oxygen species (ROS) and cytotoxicity, resulting in tissue and organ dysfunction. Numerous studies have indicated that iron overload-induced osteoporosis in mice is characterized by a reduction in volume fraction, thickness and spacing of bone trabeculae, and these findings have been corroborated in rats (4,5). Furthermore, excessive iron impedes bone formation in zebrafish models of iron overload, accompanied by decreased expression of osteoblast-specific genes, such as alkaline phosphatase (ALP), collagen type I (Col I), and Runt-related transcription factor 2 (Runx2) (6). Therefore, mouse, rat or zebrafish models subjected to iron overload may serve as valuable tools for investigating the effects of various drugs on osteoporosis.

Iron overload leading to iron toxicity is known to be closely related to amino acid, lipid and iron metabolism (7). Divalent iron exhibits strong reductive properties and can generate excessive ROS through the Fenton reaction, resulting in oxidative damage to cells (8). Mitochondria have a pivotal role in cellular metabolism, with abnormalities in the tricarboxylic acid cycle and electron transport chain being responsible for lipid peroxidation (LPO) (9). Mitochondrial ROS (mtROS) serve as indicators of mitochondrial damage, whereas lipid ROS play a pivotal role in ferroptosis (10). Oxidative mitochondrial damage induced by various external stressors, such as iron overload, can lead to various forms of cell death, including apoptosis (11). The MC3T3-E1 cells are derived from mouse embryonic skull tissue. It is an osteoblast cell line that can readily proliferate, maintain normal differentiation and osteogenic capacity in culture *in vitro*, making it a common model used for osteoporosis research (12,13). Therefore, it remains imperative to investigate whether excessive iron intervention in MC3T3-E1 cells induces mitochondrial dysfunction and apoptosis, thus impacting their differentiation into osteoblasts.

The PI3K/Akt axis is involved in the regulation of various biological processes and cellular mechanisms, such as angiogenesis (14), epigenetic regulation of tumors (15), and regulation of the nervous system and brain injury (16). Activation of the PI3K/Akt signaling pathway has been shown to inhibit ferroptosis in osteoblasts as a potential treatment for osteoporosis (17). Additionally, it has been reported that ROS act as a mediator in the regulation of the PI3K/Akt signaling pathway to safeguard osteoblasts from apoptosis and promote their osteogenesis (18,19). Arctiin (ARC), a lignin bioactive compound initially isolated from *Arctium lappa* L (20), has been demonstrated to exert antioxidant and anti-inflammatory effects (21,22). In previous studies, ARC has been reported to inhibit the migration and invasion of cervical cancer cells by regulating the PI3K/Akt signaling pathway, and to reduce inflammation by modulating macrophage polarization (23-25). ARC has also been shown to modulate osteogenic differentiation and maintain bone homeostasis in the treatment of osteoporosis (26,27). However, whether ARC can effectively treat iron overload-induced osteoporosis (IOOP) by regulating the PI3K/Akt pathway remains to be investigated.

The present study examined the efficacy of ARC in treating IOOP based on the PI3K/Akt signaling pathway. This study also aimed to provide new insights into the mechanisms via which ARC is effective in mitigating IOOP.

Materials and methods

Reagents. Penicillin/streptomycin (P/S), 0.25% Trypsin-EDTA and MC3T3-E1 mouse embryonic osteoblast precursor cells were obtained from Thermo Fisher Scientific, Inc. Fetal bovine serum (FBS) was purchased from Gibco (Thermo Fisher Scientific, Inc.). α-Minimum Essential Medium (α-MEM) and PBS were obtained from Wuhan Servicebio Technology Co., Ltd. DAPI, ferric ammonium citrate (FAC; CAS 1185-57-5), iron-dextran (CAS 9004-66-4), dimethyl sulfoxide (DMSO; CAS 67-68-5), 0.2% Triton X-100 and Immobilon® transfer membrane (PVDF membrane) were purchased from MilliporeSigma. LY294002 (CAS 154447-36-6) was obtained from MedChemExpress. ARC (HPLC ≥98%, CAS 20362-31-6) was obtained from Chengdu Desite Biotechnology Co., Ltd., which was dissolved in DMSO as stock solution and stored at -20˚C in a light-proof environment. The concentration of DMSO in the cell culture reagents was <0.1%. Alizarin Red S (ARS) Solution was purchased from OriCell Therapeutics, Co., Ltd. RIPA buffer, MitoSOX Red Mitochondrial Superoxide Indicator, dichlorodihydrofluorescein diacetate (DCFH-DA), LPO sensor (BODIPY® C11), the BCIP/NBT ALP Color Development Kit (cat. no. C3202), BCA Assay Kit, SDS-PAGE Gel Preparation Kit and the Membrane Potential Assay Kit (JC-1) were all from Beyotime Institute of Biotechnology. Cell Counting Kit 8 (CCK8) and Calcein-AM were from GlpBio Technology. ECL Chemiluminescent Substrate Substrate (Extra Ultra Sensitive) Kit was obtained from Biosharp Life Sciences. The Annexin V-FITC/PI Kit was purchased from Multi Sciences (Lianke) Biotechnology Co., Ltd. The hematoxylin and eosin (H&E) staining kit, membrane regeneration solution reagent and Serum Iron Concentration Assay Kit (cat. no. BC1735) were from Beijing Solarbio Science & Technology Co., Ltd. The following western blotting primary antibodies were obtained from Affinity Biosciences: Col I (cat. no. AF7001), Runx2 (cat. no. AF5186), Bax (cat. no. AF0120), Bcl-2 (cat. no. AF6139), PI3K (cat. no. AF6241), phosphorylated (p)-PI3K (cat. no. AF3242), Akt (cat. no. AF6261), p-Akt (cat. no. AF0016), β-actin (cat. no. AF7018). Goat anti-rabbit IgG H&L secondary antibody (cat. no. bs-40295G-HRP) was purchased from BIOSS.

Animal experiments. A total of 40 male C57/BL6 mice (age, 49 days; weight, 20±2 g) were provided by The Animal Experiment Center of Guangzhou University of Chinese Medicine (Guangzhou, China). The temperature of the animal laboratory is controlled at 20-26˚C, with a daily temperature difference of 4˚C. The relative humidity is controlled at 40-70%. The mice had constant access to adequate SPF-grade mouse chow and water and were maintained under a 12-h light/dark cycle. After 7 days of acclimatization, the mice were randomly divided into the following four groups: i) Control group, where mice received a once weekly intraperitoneal injection of saline equivalent to the volume of iron dextrose applied + a daily gavage of saline equivalent to the volume to the ARC applied (n=6); ii) intraperitoneal injection of dextran iron (ID) group, where mice received a once weekly intraperitoneal injection of dextran iron + a daily gavage of equivalent volume of saline (n=6); iii) ID + ARC-L group,

where the mice received a weekly intraperitoneal injection of dextran iron + a daily gavage of 20 mg/kg ARC (n=6); and iv) ID + ARC-H group, where the mice received a weekly intraperitoneal injection of dextran iron + a daily gavage of 40 mg/kg ARC (n=6). *In vivo* doses of ARC were obtained with reference to previous literature (28,29). All mice, with the exception of those in the normal control group, were administered intraperitoneal doses of 500 mg/kg iron dextran for 3 months. In particular, dextran iron is administered intraperitoneally 1 month prior to ARC gavage (30). The design of the animal experiment protocols in the present study is shown in Fig. 1A. All mice used in the present study were raised in the SPF Experimental Animal Center of the First Affiliated Hospital of Guangzhou University of Chinese Medicine (Guangzhou, China). All animal experiments were approved by the Ethics Committee of Guangzhou University of Chinese Medicine (approval no. TCMF1-2021029; May 20, 2021). Animals were euthanized at 20 weeks of age through an intraperitoneal injection of an overdose of pentobarbital (150 mg/kg). Death was confirmed by continuing to observe the mice for 2 min after the observation of no heartbeat, respiration and the pupils are dilated.

Micro-computed tomography (micro-CT) analysis. The left tibiae of mice after euthanasia from the aforementioned pentobarbital protocol were collected and fixed in 4% paraformaldehyde for 24 h at room temperature before being scanning with the Skyscan 1172 micro-CT system (Bruker Corporation). Subsequently, the data were analyzed using a custom analysis program (version 1.17.7.2+; CTAn Skyscan; Bruker Corporation). From the cross marker below the tibial plateau, the volume of interest consists primarily of a 100-layer transverse section. Bone microstructural parameters, such as structure model index (SMI; SMI=Skeletal Muscle Area (SMA)/height^2; SMA was calculated and analyzed from CT images.), ratio of bone volume/tissue volume (BV/TV), trabecular thickness (Tb.Th), trabecular separation (Tb.Sp), trabecular number (Tb.N) and trabecular bone pattern factor (Tb.Pf) were analyzed according to the manufacturer's protocol.

H&E staining assay. The aforementioned fixed samples were decalcified in 14% EDTA at 37˚C for 1 week. After decalcification, the samples were embedded in paraffin and cut into 5-μm sections. The sections were stained with hematoxylin for 5 min and eosin stain for 1 min, both at room temperature, before and a panoramic digital slide scanner (3DHISTECH Ltd.) was used to assess them.

Immunohistochemistry. The aforementioned paraffin-embedded tissues were sectioned into 5-μm thin slices, before the slides were fished out and placed in a 37˚C constant-temperature drying oven for 12 h. The dried slides were sequentially deparaffinized by immersion in xylene solution followed by a decreasing ethanol gradient, before being washed with distilled water and PBS. The sections were then added to a boiling (100˚C) citrate antigen retrieval solution (Beyotime Institute of Biotechnology) for 15 min, prior to cooling and incubation with 3% H_2O_2 for 5 min at room temperature to inactivate endogenous peroxidase. The sections were then blocked with 10% goat serum (Beyotime Institute of Biotechnology) for 30 min at room temperature. The blocked sections were then incubated with primary antibodies (all 1:200) against p-PI3K (cat. no. AF3242; Affinity Biosciences), Col I (cat. no. AF7001; Affinity Biosciences) or Runx2 (cat. no. AF5186; Affinity Biosciences) overnight at 4˚C, followed by incubation with HRP-labeled Goat Anti-Rabbit IgG secondary antibodies (1:50; cat. no. A0208; Beyotime Institute of Biotechnology) for 2 h at room temperature. The configured DAB coloring solution (20X DAB Substrate Kit; cat. no. BL732A; Biosharp Life Sciences) was then added dropwise to the slides according to the manufacturer's protocol and the staining results were observed under a microscope. The slides were then rinsed with PBS. Counterstaining was performed with hematoxylin for 1 min at room temperature, the tissue was sealed with neutral gum and images were captured under a light microscope.

Serum iron concentration assay. A total of 125 μl of each of the Serum Iron Concentration Assay Kit Reagents 1 and 2 was added to each tube. Subsequently, 125 μl distilled water was added to a blank tube, before 125 μl serum [1 week before euthanasia, 0.3 ml of blood was withdrawn once from the submandibular vein of the mice (31)], which was let stand for 1 h and then centrifuged at 2,500 x g for 10 min at 4˚C to isolate the supernatant) to be tested was added to the assay tube, and 125 μl standard solution (from the kit) was added to the standard tube. Subsequently, the tubes were centrifuged at 10,000 x g for 10 min at room temperature to obtain the supernatants, the absorbance of which was measured at 520 nm using a microplate reader (Thermo Fisher Scientific, Inc.). Finally, serum iron concentration was calculated using the following formula: Serum iron content (μg/ml)=125 x (assay tube-distilled water tube)/(standard tube-distilled water tube).

Cell culture and experimental protocol. MC3T3-E1 cells were cultured in α-MEM containing 10% FBS and 1% P/S in a 37˚C cell culture incubator with 5% CO_2. Cells were harvested when they reached ~80% confluence and underwent drug (FAC, ARC and LY294002) intervention for 48 h at 37˚C prior to further experimentation. FAC was prepared as a 100 mM master mix with PBS, whereas ARC and LY294002 were prepared as a 10 mM concentration with DMSO. All drugs were stored at -20˚C. All *in vitro* experiments were repeated three times.

CCK8 cell viability assay. CCK8 assay was performed to assess the effect of ARC on cell viability. After treating MC3T3-E1 cells (In 96-well plate at a density of 5x10^3 cells per well) with different concentrations of ARC (0, 2, 4, 8, 12, 16 and 20 μM) for 48 h, 100 μl CCK8 working solution (containing 10 μl CCK8 reagent and 90 μl serum-free medium) was added to each well and incubated for 2 h at 37˚C in the aforementioned cell culture environment. The absorbance was then measured at 450 nm using a microplate reader (Thermo Fisher Scientific, Inc.). To determine the appropriate dose of FAC, cells in 96-well plates were treated with different concentrations of FAC (0, 20, 40, 60, 80, 100, 200, 300, 400 and 500 μM) for 48 h at 37˚C and the CCK8 assay was performed as aforementioned. The final cellular intervention dose of FAC was determined to be 500 μM. Subsequently, to

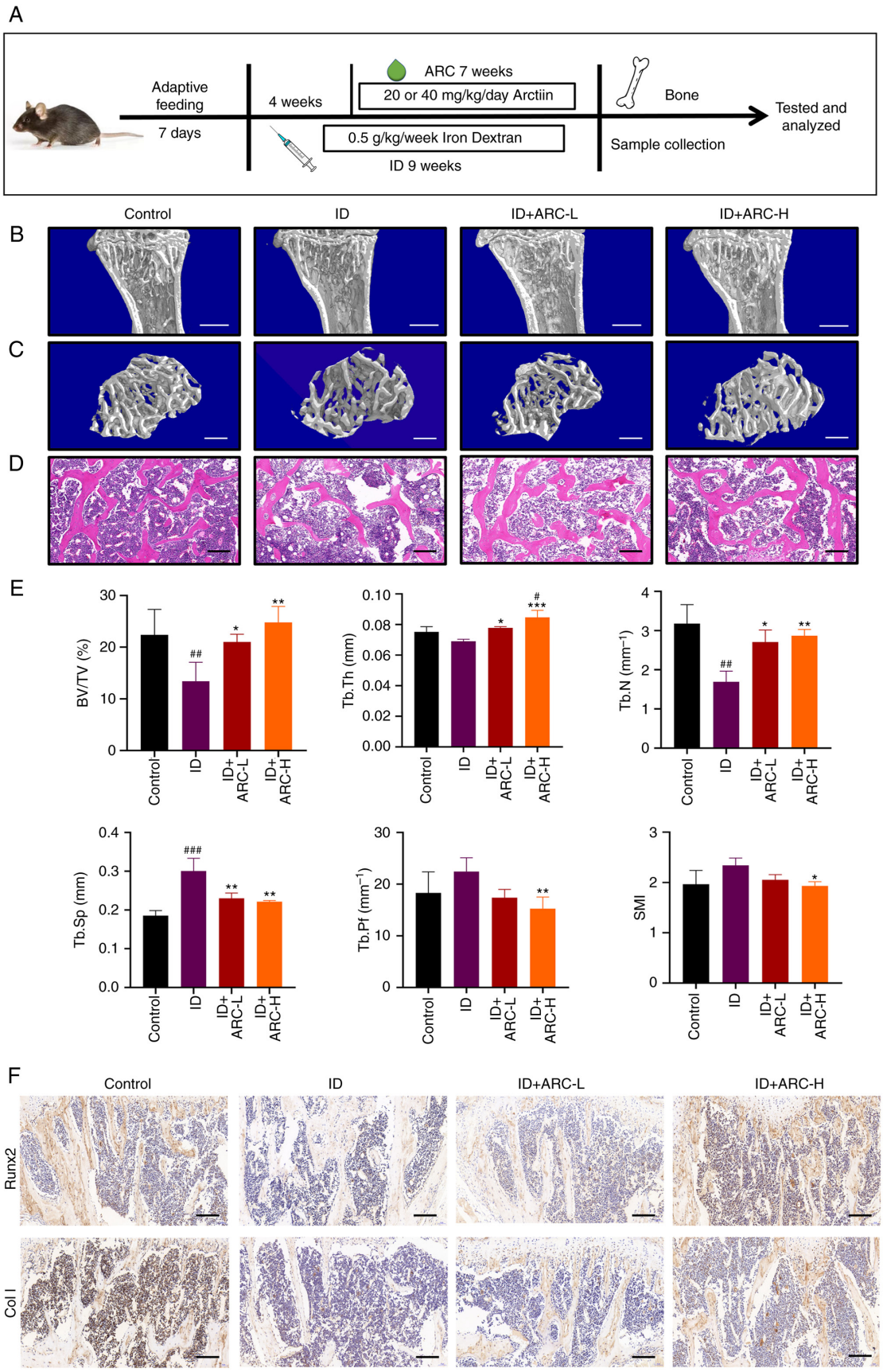

Figure 1. ARC alleviates IOOP in mice. (A) Modeling method and flow chart of ARC treatment in a mouse model of IOOP. (B and C) Micro-CT analysis of tibial specimens. Scale bars: (B) 1 mm and (C) 0.5 mm. (D) Hematoxylin and eosin staining of excised thin layers of tibial specimens. Scale bar, 0.2 mm. (E) Bone structural parameters obtained from micro-CT scans, including SMI, BV/TV, Tb.Th, Tb.Sp, Tb.N and Tb.Pf, were analyzed. (F) Immunohistochemical analysis of Runx2 and Col I in tibial samples. Scale bar, 0.2 mm. Data are presented as the mean ± SD. ***P<0.001, **P<0.01 and *P<0.05 vs. ID; $^{###}$P<0.001, $^{##}$P<0.01 and $^{#}$P<0.05 vs. Con. ARC, arctiin; Con, control; ARC-H, ARC-high; ARC-L, ARC-low; BV/TV, bone volume/tissue volume; Col I, collagen type I; ID, dextran iron; Runx2, Runt-related transcription factor 2; SMI, structure model index; Tb.N, trabecular bone number; Tb.Pf, trabecular bone pattern factor; Tb.Sp, trabecular separation/spacing; Tb.Th, trabecular thickness; micro-CT, micro-computed tomography.

determine the appropriate dosage of ARC, cells in 96-well plates were treated with 500 μM FAC and various concentrations of ARC (0, 2, 4, 6, 8, 10 and 12 μM) for 48 h at 37˚C and the CCK8 assay was performed as aforementioned.

Grouping of cytology experiments. The following groups were set up for cytology experiments: i) Control group, where cells were cultured in α-MEM medium containing 10% FBS; ii) FAC group, where cells were cultured in α-MEM medium containing 10% FBS and 500 μM FAC; iii) FAC + ARC-L group, where cells were cultured in α-MEM medium containing 10% FBS, 500 μM FAC and 4 μM ARC; abd iv) FAC + ARC-H group, where cells were cultured with α-MEM medium containing 10% FBS, 500 μM FAC and 8 μM ARC.

Calcein AM assay of intracellular iron content. The calcein AM staining stock solution was diluted to a working solution at a concentration of 2 μM in serum-free medium. MC3T3-E1 cells were inoculated into 24-well plates at a density of $3x10^4$ overnight at 37˚C to stabilize cell proliferation and were then cultured for 48 h at 37˚C in 10% FBS-containing medium containing FAC (500 μM), with or without ARC (4 and 8 μM). FAC and ARC were added to α-MEM containing 10% FBS at 37˚C. Cells were washed twice with PBS and were then incubated with calcein AM working solution for 30 min at 37˚C in the dark. The cells were washed twice with PBS, and were then observed and photographed using a fluorescence microscope (Leica Microsystems, Inc.) under an emission light wavelength of 494-514 nm.

Analysis of bone mineralization. MC3T3-E1 cells were seeded at a density of $3x10^4$ in 24-well plates at 30% confluence overnight at 37˚C in normal α-MEM and were then cultured in osteoblast differentiation medium containing 1 μM dexamethasone, 100 μg/ml ascorbic acid and 10 mM β-glycerophosphate, with ARC (4 or 8 μM) and with or without FAC for 7 and 21 days at 37˚C (medium changed every 3 days). Subsequently, cells underwent ALP staining (BCIP/NBT ALP Color Development Kit) and ARS staining. Briefly, cells were fixed in 4% paraformaldehyde for 20 min at room temperature before staining, washed twice with double distilled water and then stained with the BCIP/NBT working solution (500 μl) or ARS solution (500 μl) for 2 h at room temperature. The staining signals were then recorded using light microscopy accordingly.

Apoptosis detection assay. Cells were cultured for 48 h at 37˚C in 10% FBS-containing medium containing FAC (500 μM), with or without ARC (4 and 8 μM). Apoptosis was then analyzed using the Annexin V-FITC/PI Kit. Cells were washed with PBS after digestion with 0.25% Trypsin-EDTA for 2 min at 37˚C. In the dark, cells (each aliquot contains ~$3x10^5$ cells) were incubated with Annexin V-FITC and PI for 5 min at room temperature (Each aliquot of staining contains 5 μl V-FITC and 10 μl PI). A BD FACSCanto II flow cytometer (BD Biosciences) was then used to detect the cells. The resulting data were processed by BD FACSDiva™ software (V9.0; BD Biosciences) and the FlowJo software (V10.6.2; BD Biosciences).

Assessment of ROS levels. After cell treatment [cultured for 48 h at 37˚C in 10% FBS-containing medium-containing FAC (500 μM), with or without ARC (4 and 8 μM)], the cells were incubated for 20 min at 37˚C in the dark with serum-free medium containing DCFH-DA, BODIPY C11 or MitoSOX Red Mitochondrial Superoxide Indicator-probe (DCFH-DA and BODIPY C11 at a working concentration of 10 μM and MitoSOX Red Mitochondrial Superoxide Indicator at a working concentration of 200 nM). The cells were then washed twice with PBS, before intracellular ROS, lipid ROS or mtROS fluorescence intensity were detected using a fluorescence microscope. Alternatively, cells were digested and incubated with the probe for detection by flow cytometry, using the same flow cytometer and software as that for Annexin V-FITC/PI assay.

Mitochondrial membrane potential (MMP) measurements. The harvested cells [The harvested cells were from 6-well plates with $2x10^5$ cells per well. They were first cultured for 48 h at 37˚C in 10% FBS-containing medium containing FAC (500 μM), with or without ARC (4 and 8 μM)] were washed twice with PBS, before they were incubated directly with the JC-1 working solution (the concentration of JC-1 working solution was 10 μg/ml) for 20 min at 37˚C in the dark or were digested with 0.25% Trypsin-EDTA and then incubated with JC-1 for 20 min. Subsequently, the cells were washed twice and MMP was examined by fluorescence microscopy or flow cytometry (as aforementioned), respectively.

Immunofluorescence. For permeabilization, the cells [cultured for 48 h at 37˚C in 10% FBS-containing medium containing FAC (500 μM), with or without ARC (4 and 8 μM)] were fixed for 15 min at room temperature with 4% paraformaldehyde, then treated with 0.2% Triton X-100 for 30 min at room temperature and blocked with 1% BSA (Biosharp Life Sciences)/10% normal goat serum (Beyotime Institute of Biotechnology)/0.3 glycine in 0.1% PBS-Tween for 1 h at room temperature. After incubation with the anti-p-PI3K primary antibody (1:200; cat. no. AF3242; Affinity Biosciences) overnight at 4˚C, the cells were incubated with a goat anti-rabbit IgG H&L (Alexa Fluor® 647) secondary antibody (cat. no. ab150083, abcam) for 1 h at room temperature. The secondary antibody was prepared in a 1:200 ratio with 4% BSA. The nuclei were stained with DAPI (the working concentration was 1 μg/ml) for 3 min at room temperature. Confocal laser scanning microscopy was used to obtain the immunofluorescence images.

Western blotting. Total protein was extracted from the treated MC3T3-E1 cells [cultured for 48 h in 10% FBS-containing medium containing FAC (500 μM), with or without ARC (4 and 8 μM)] using RIPA buffer containing phosphatase inhibitor and universal protease inhibitor, and the protein concentration was determined using a BCA assay kit. Subsequently, proteins (20 μg) were separated by SDS-PAGE on 10% gels and were transferred onto PVDF membranes, which were blocked with Quick Blocking Solution (Beyotime Institute of Biotechnology) for 15 min at room temperature according to the manufacturer's protocol. The membranes were then incubated overnight at 4˚C with primary antibodies (Col I, Runx2, p-PI3K, PI3K, p-Akt, Akt, Bax, Bcl-2, β-actin; all 1:1,000). The membranes were subsequently washed with

TBS-10% Tween (Beyotime Institute of Biotechnology) and incubated with the corresponding HRP-conjugated secondary IgG antibodies (1:5,000) for 1 h at room temperature. Protein strips that had been coated with secondary antibodies were cut horizontally according to the protocol of Dual Color Standards (Used to provide standard protein molecular weights; Bio-Rad Laboratories, Inc.), and were subsequently visualized with the ECL Chemiluminescent Substrate Substrate (Extra Ultra Sensitive) Kit and a gel imaging system (Bio-Rad Laboratories, Inc.). The grayscale values were semi-quantified using the ImageJ (V.1.8.0-172) software (National Institutes of Health). The PI3K and Akt blots were washed with membrane regeneration reagent at room temperature for 10 min to wash off the primary and secondary antibodies, followed by re-analysis with the p-PI3K and p-Akt antibodies as aforementioned.

Statistical analysis. Results are from at least three different experiments. Mean values are presented as the mean ± SD. Statistical analysis was performed using SPSS (V25.0) software (IBM Corp). One-way ANOVA and Tukey's post hoc test (By SPSS) were used to compare three or more groups. $P<0.05$ was considered to indicate a statistically significant difference. All graphs were generated using GraphPad Prism (version 9.0.2; Dotmatics).

Results

ARC alleviates IOOP in mice. To investigate the effect of ARC on IOOP *in vivo*, micro-CT was performed. Notably, micro-CT analysis showed that mice in the ID group had severe bone loss, thin and disorganized bone trabeculae and enlarged bone marrow cavities compared with the control group. By contrast, after gavage of ARC, the bone mass of mice was restored to some extent and approached that of the control group (Fig. 1B and C). The data from the micro-CT scans were then analyzed, and the two ARC groups exhibited an increase in BV/TV, Tb.Th and Tb.N, and a decrease in SMI, Tb.Sp and Tb.Pf compared with those in the ID group (Fig. 1E). These results were promising and some of the effects were even better in the ARC-H group than in the control group. Furthermore, after ARC treatment, H&E staining showed a more pronounced reduction in adipocytes, recovery of the bone marrow cavity and more orderly bone trabeculae (Fig. 1D). Immunohistochemistry can detect the effects of drugs on *in vivo* indicators, and the present study examined Runx2 and Col I, which promote osteogenesis (32,33). The results showed that mice in the ARC groups exhibited increased Runx2 and Col I expression in the bone trabeculae and bone marrow compared with that in the ID group (Fig. 1F). These results suggested that ARC may have the ability to counteract bone loss caused by iron overload.

ARC dose-dependently affects the viability of MC3T3-E1 cells. The chemical structural formula of ARC is shown in Fig. 2A. The effect of ARC on MC3T3-E1 cell viability was examined using the CCK8 assay, and the results showed that MC3T3-E1 cells exhibited the best viability when the concentration of ARC was between 2 and 12 μM (Fig. 2B); in this concentration range, ARC had a clear dose-dependent effect on viability. Notably, slight toxicity to cells was observed when the ARC concentration exceeded 16 μM. In addition, MC3T3-E1 cells were treated with different concentrations of FAC to create a model of intracellular iron overload. The results showed that low doses of FAC were able to promote cell viability though significance was not reached, whereas cell viability began to decline when FAC concentration exceeded 200 μM, and decreased by ~50% when FAC concentration reached 500 μM. Therefore, 500 μM FAC was selected as the appropriate concentration for intracellular iron overload (Fig. 2C). After the iron overload model was constructed, cell viability was significantly decreased, and this decrease was reversed by ARC at concentrations of 2-8 μM (Fig. 2D). Based on these results, it was indicated that ARC may be able to affect cellular viability in a dose-dependent manner.

ARC reduces intracellular iron concentration. Intracellular iron concentration was examined according to the method of Ma *et al* (34). Intracellular Fe^{3+} is able to quench the fluorescent system by complexing with calcein AM. Therefore, there is an inverse relationship between intracellular iron ion concentration and fluorescence intensity. Compared with that in the control group, the intensity of cellular fluorescence was greatly reduced in the FAC group, suggesting a significant increase in intracellular iron content. ARC was able to promote intracellular iron ion excretion. However, iron concentrations in the ARC group were still significantly higher compared with those in the control group (Fig. 3A and B). The fluorescence intensity of the FAC group was markedly lower compared with that of the FAC + ARC-L/H group, suggesting that more Fe^{3+} was present in the FAC group. This finding suggested that although ARC could reduce iron accumulation in iron-overloaded MC3T3-E1 cells, it is difficult to restore iron concentration to normal levels. *In vivo*, serum iron concentrations in mice in the ID group were similarly significantly higher compared with those in the control group. Serum iron concentrations in mice in the ID + ARC group were lower compared with those in the ID group, even though it was difficult to restore them to normal group levels (Fig. S1).

ARC attenuates the inhibitory effect of iron overload on the osteogenesis of MC3T3-E1 cells. To investigate the effect of ARC on the osteogenesis of MC3T3-E1 cells, cells were cultured for 7 days in osteoblast differentiation medium containing 1 μM dexamethasone, 100 μg/ml ascorbic acid and 10 mM β-glycerophosphate with ARC (4 or 8 μM) with or without FAC at 37˚C. Staining with the BCIP/NBT ALP Staining Kit showed that FAC significantly inhibited the osteogenic potential of MC3T3-E1 cells; although the difference in effect between the two concentrations of ARC was not significant, both were able to significantly reverse the effects of FAC (Fig. 4A and D). Subsequently, cells were cultured for 21 days and the formation of calcium deposits was assessed by ARS staining; the obtained results were consistent with those of ALP staining (Fig. 4B and E). The expression levels of osteogenic-related proteins (Runx2 and Col I) were then detected in cells cultured with normal α-MEM by western blotting. The expression levels of Col I and Runx2 were significantly reduced in the model group, a trend that was alleviated after ARC treatment (Fig. 4C, F and G). Based on these results, it may be suggested that ARC could reduce the iron overload-induced inhibition of MC3T3-E1 cell osteogenesis.

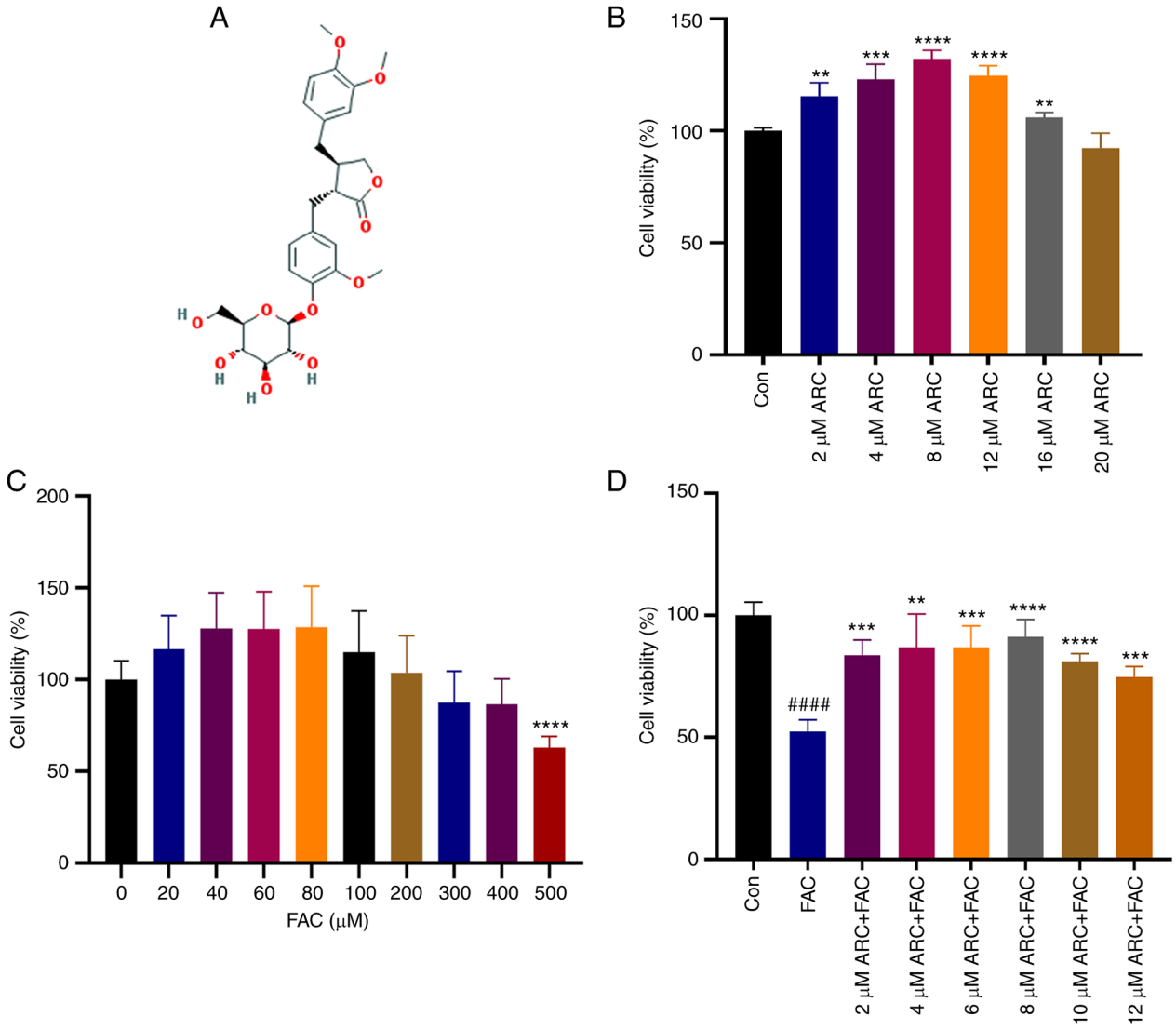

Figure 2. ARC dose-dependently affects the viability of MC3T3-E1 cells. (A) Chemical formula of ARC. MC3T3-E1 cells were treated with (B) different concentrations of ARC (C) different concentrations of FAC, or (D) different concentrations of ARC with or without FAC for 48 h, and then cell viability was determined using using Cell Counting Kit 8. Data are presented as the mean ± SD. ****P<0.0001, ***P<0.001 and **P<0.01 vs. Con (B), 0 μm (C) or FAC (D); $^{\#\#\#\#}$P<0.0001 vs. Con (D). ARC, arctiin; Con, control; FAC, ferric ammonium citrate.

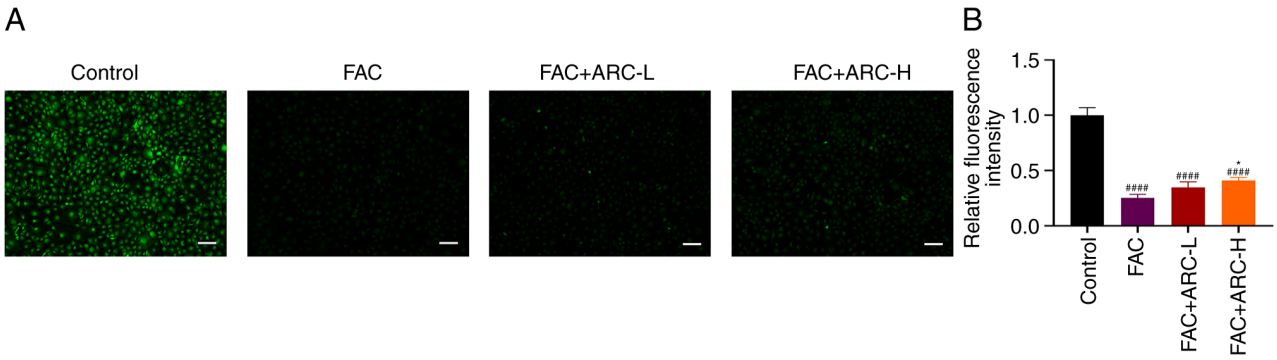

Figure 3. ARC reduces intracellular iron concentration. (A) MC3T3-E1 cells were incubated with calcein AM and fluorescence images were taken by confocal microscopy. (B) Relative fluorescence intensity. Scale bar, 100 μm. Data are presented as the mean ± SD. *P<0.05 vs. Mod; $^{\#\#\#\#}$P<0.0001 vs. Con. ARC, arctiin; ARC-H, ARC-high; ARC-L, ARC-low; Con, control; FAC, ferric ammonium citrate; Mod, model.

ARC reduces iron overload-induced apoptosis in MC3T3-E1 cells. Annexin V-FITC/PI staining was performed to further verify whether ARC had a protective effect against apoptosis in MC3T3-E1 cells following high-dose FAC treatment. The results showed that apoptosis was markedly increased in the iron overload model compared with that in the control

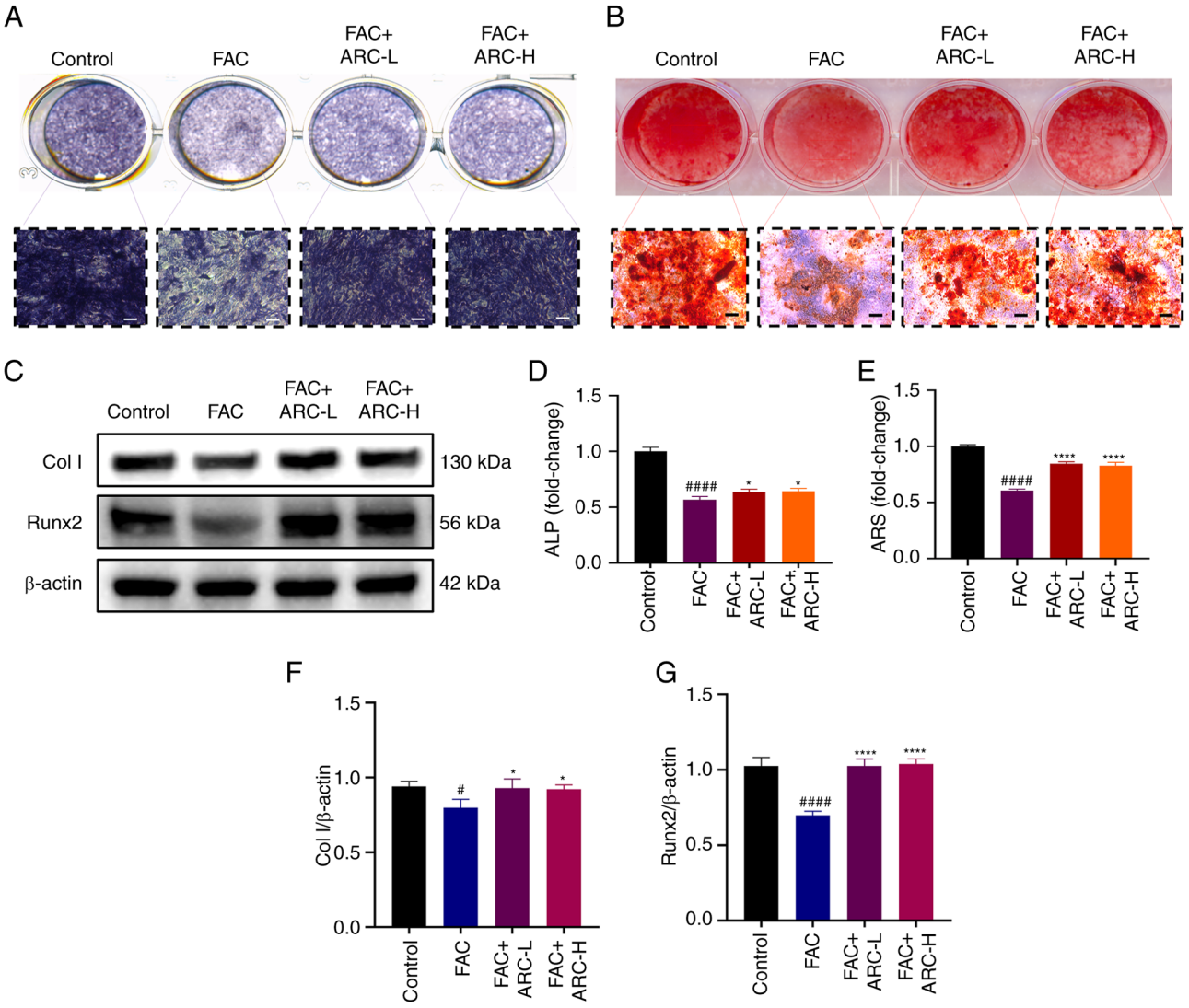

Figure 4. ARC attenuates the inhibitory effect of iron overload on MC3T3-E1 cell osteogenesis. After FAC treatment, with or without ARC treatment, MC3T3-E1 cells were cultured in an osteogenic induction medium containing FAC/ARC treatment and stained with (A) ALP or (B) ARS on days 7 and 21, respectively. Scale bar, 100 μm. (C) MC3T3-E1 cells were harvested after treatment with FAC with or without ARC intervention for 48 h, before Col I and Runx2 expression levels were measured by western blotting. (D) Ratio of area of purple nodules of calcium phosphate to total area after staining. (E) Mineralized nodules were determined by calculating the ratio of mineralized area to total area after staining. Expression levels of (F) Col I and (G) Runx2 were semi-quantified by western blotting. Data are presented as the mean ± SD. ****P<0.0001 and *P<0.05 vs. Mod; $^{\#\#\#\#}$P<0.0001 and $^{\#}$P<0.05 vs. Con. ALP, alkaline phosphatase; ARC, arctiin; ARC-H, ARC-high; ARC-L, ARC-low; ARS, Alizarin Red S; Col I, collagen type I; Con, control; FAC, ferric ammonium citrate; Mod, model (500 μM FAC); Runx2, Runt-related transcription factor 2.

group, with the rate of late apoptosis increasing from ~8 to ~25% of cells (Fig. 5A and B). By contrast, ARC treatment, especially at a high concentration, was able to reduce the apoptotic rate of cells by ~50% compared with that in the model group, thus significantly attenuating the apoptotic effect of iron overload on MC3T3-E1 cells. The detection of apoptosis marker proteins Bcl-2 and Bax by western blotting further verified that Bcl-2 expression was reduced and Bax expression increased following intervention with FAC, whereas ARC was able to reverse these effects (Fig. 5C-E). Based on these results, it was indicated that ARC was able to attenuate the apoptosis of MC3T3-E1 cells caused by excess FAC.

ARC reduces iron overload-induced mitochondrial damage. When cells are exposed to stimuli (including the accumulation of oxidants), mitochondria inevitably initiate a stress response. The ability to respond appropriately to this stimulus determines two different consequences for mitochondria. When mitochondrial function is dysfunctional, it affects the MMP and accelerates apoptosis (11). Therefore, the present study next examined MMP using the JC-1 assay to assess mitochondrial function and to determine whether ARC inhibits MMP collapse. The results showed that after induction of iron overload, the green fluorescence intensity of JC-1 monomers increased and the red fluorescence intensity of JC-1 aggregates decreased, indicating that MMP was decreased and mitochondrial function was impaired at this time (Fig. 6A). Notably, when mitochondrial function is in a dysregulated state, this indicates that the cell is in a dysregulated state of oxidant accumulation. Notably, the results of the ARC-L group and ARC-H group were similar to those of the control group, suggesting

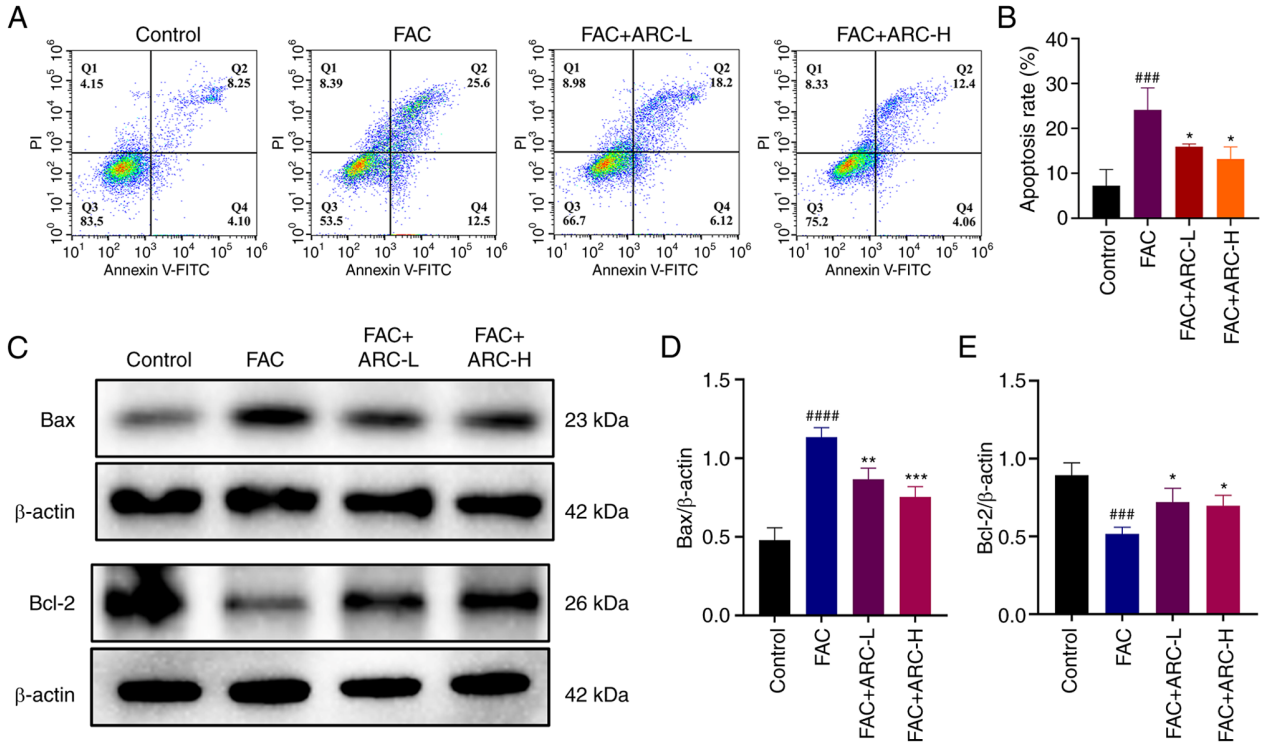

Figure 5. ARC reduces iron overload-induced apoptosis in MC3T3-E1 cells. (A) After treatment with FAC with or without ARC for 48 h, Annexin V-FITC/PI staining was performed and apoptosis was assessed by flow cytometry. (B) Statistical analysis of percentage of late apoptosis (Q2) in each group. (C-E) MC3T3-E1 cells were harvested after treatment with FAC with or without ARC for 48 h, and Bcl-2 and Bax expression levels were measured by western blotting. Data are presented as the mean ± SD. ***P<0.001, **P<0.01 and *P<0.05 vs. Con; $^{####}$P<0.0001 and $^{###}$P<0.001 vs. Mod. ARC, arctiin; ARC-H, ARC-high; ARC-L, ARC-low; Con, control; FAC, ferric ammonium citrate; Mod, model (500 μM FAC).

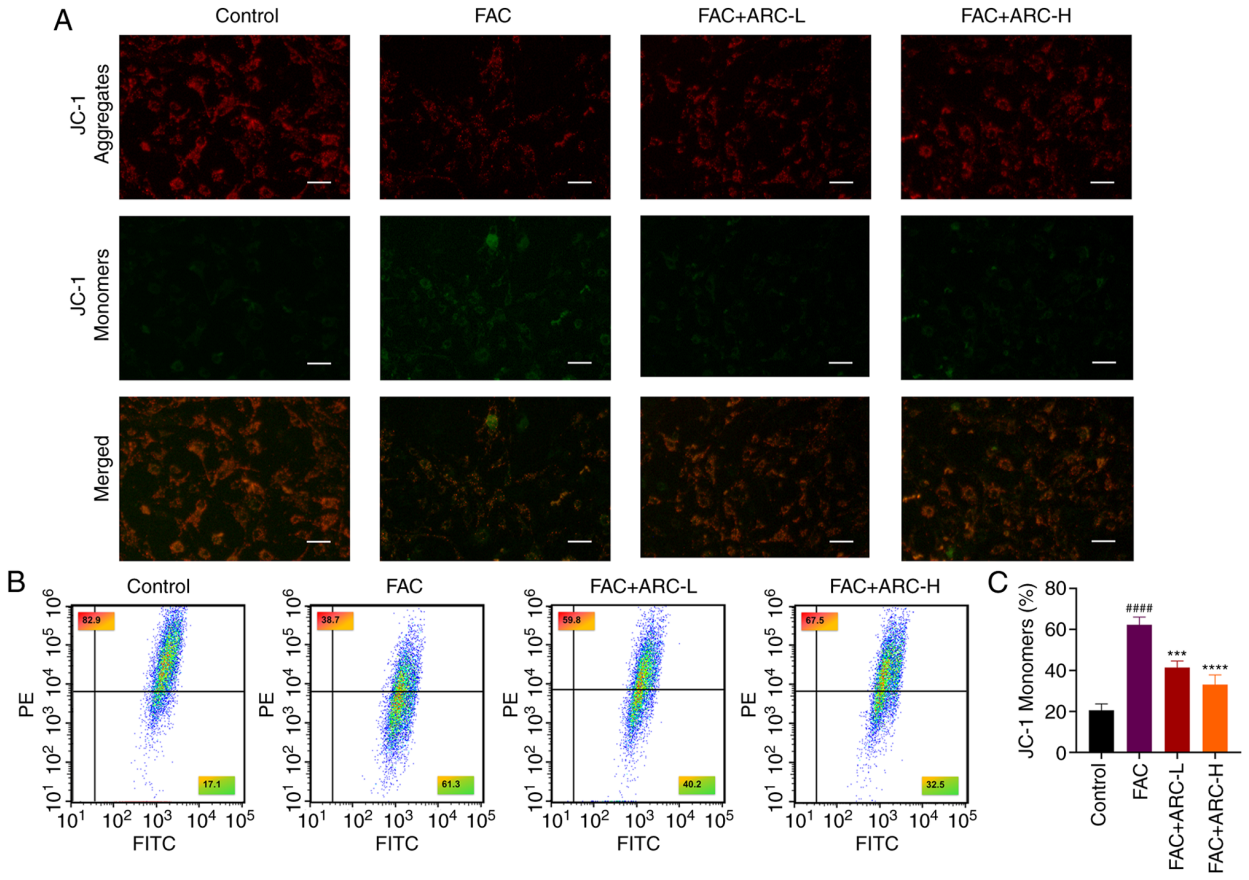

Figure 6. ARC reduces iron overload-induced mitochondrial damage. (A) JC-1 fluorescence staining of cells was observed by confocal microscopy. Scale bar, 50 μm. (B) JC-1 fluorescence staining of cells was observed by flow cytomrtry. (C) Quantification of JC-1 monomers. Data are presented as the mean ± SD. ****P<0.0001 and ***P<0.001 vs. Mod; $^{####}$P<0.0001 vs. Con. ARC, arctiin; ARC-H, ARC-high; ARC-L, ARC-low; Con, control; FAC, ferric ammonium citrate; Mod, model (500 μM FAC).

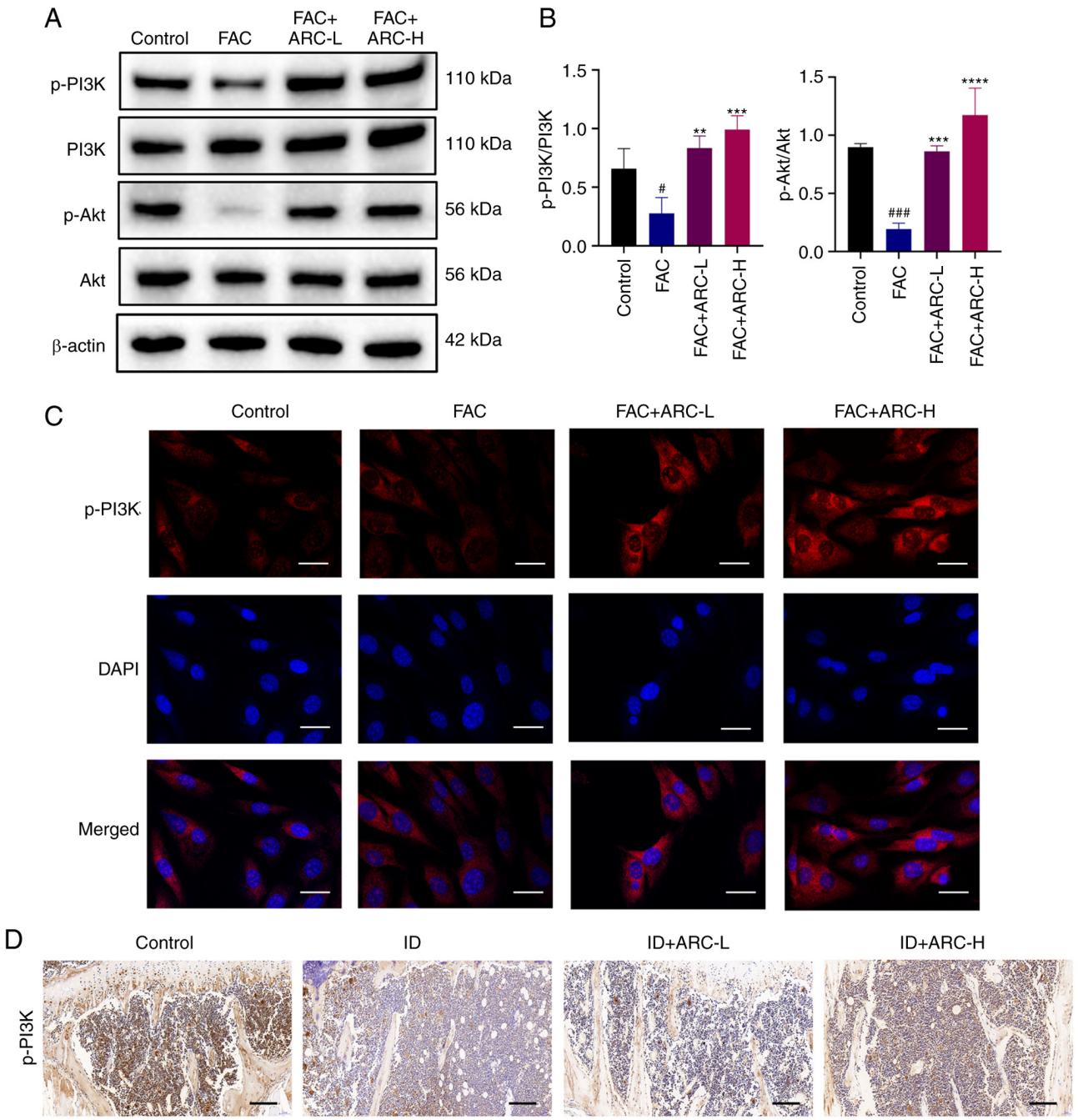

Figure 7. ARC induces activation of the PI3K/Akt pathway in iron overload-induced MC3T3-E1 cells. (A) Expression levels of p-PI3K/PI3K and Akt/p-Akt were analyzed by western blotting. (B) Statistical analysis of blots. (C) Immunofluorescence analysis of p-PI3K (red) and DAPI-stained nuclear fluorescence (blue) were visualized by confocal microscopy. Scale bar, 5 μm. (D) Thin layers of tibial specimens were immunohistochemically stained for p-PI3K. Scale bar, 0.2 mm. Data are presented as the mean ± SD. ****P<0.0001, ***P<0.001 and **P<0.01 vs. Mod; $^{###}$P<0.001 and $^{#}$P<0.05 vs. Con. Con. ARC, arctiin; ARC-H, ARC-high; ARC-L, ARC-low; Con, control; FAC, ferric ammonium citrate; ID, dextran iron; Mod, model (500 μM FAC); p-, phosphorylated.

that a high concentration of ARC was able to improve these conditions. The present study verified the changes in MMP by flow cytometry; the obtained results were consistent with those observed under microscopy (Fig. 6B and C). Taken together, ARC improved the mitochondrial function affected by excess FAC.

ARC activates the PI3K/Akt pathway in iron overload-induced MC3T3-E1 cells. The effect of ARC on the PI3K/Akt pathway in MC3T3-E1 cells after FAC treatment was detected by western blotting and immunofluorescence. Notably, PI3K/Akt pathway phosphorylation was significantly inhibited after FAC treatment; however, ARC was able to significantly activate their phosphorylation (Fig. 7A and B). Subsequent *in vitro* immunofluorescence and *in vivo* immunohistochemistry analyses of p-PI3K verified these results (Fig. 7C and D).

To further validate the effect of ARC on the PI3K/Akt pathway, the PI3K/Akt pathway inhibitor LY294002 was used for reverse validation. Following treatment with LY294002, the ARC-induced phosphorylation of the PI3K/Akt pathway, and expression of the osteogenic marker proteins Col I and Runx2 and anti-apoptotic protein Bcl-2 were again inhibited

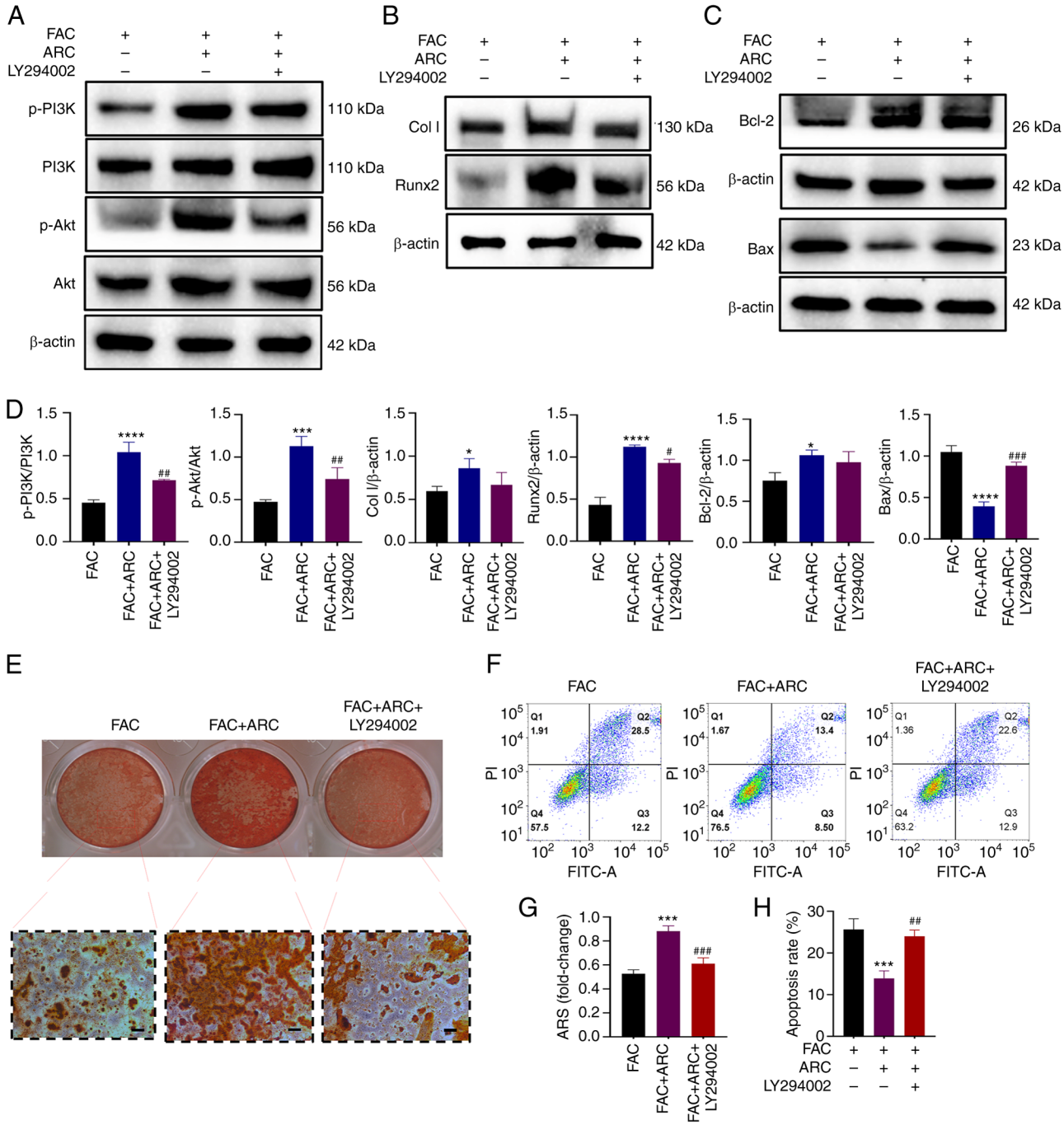

Figure 8. PI3K pathway inhibitors can impair the anti-apoptotic and bone-producing abilities of ARC. (A) Expression levels of p-PI3K/PI3K, Akt/p-Akt were analyzed by western blotting. (B) Expression levels of Col I and Runx2 were analyzed by western blotting. (C) Expression levels of Bcl-2 and Bax were analyzed by western blotting. (D) Statistical analysis of blots. (E) After FAC treatment, with or without ARC and LY294002, MC3T3-E1 cells were cultured in an osteogenic induction medium containing FAC/ARC and stained with ARS on day 21. Scale bar, 100 μm. (F) Cells were treated with FAC for 48 h with or without ARC and LY294002 intervention, after which Annexin V-FITC/PI staining was performed to detect apoptosis. (G) Mineralized nodules were quantified by calculating the ratio of mineralized area to total area after staining. (H) Statistical analysis of percentage of late apoptosis (Q2) in (F) Data are presented as the mean ± SD. ****P<0.0001, ***P<0.001 and *P<0.05 vs. FAC; $^{###}$P<0.001, $^{##}$P<0.01 and $^{#}$P<0.05 vs. FAC + ARC. ARC, arctiin; ARS, Alizarin Red S; Col I, collagen type I; FAC, ferric ammonium citrate; p-, phosphorylated; Runx2, Runt-related transcription factor 2.

(Fig. 8A-D). By contrast, the apoptosis marker protein Bax, which was reduced by ARC, was increased by LY294002 (Fig. 8C and D). Subsequently, the osteogenic capacity of cells was assessed, and ARS staining showed that treatment with LY294002 further reduced the ability of MC3T3-E1 cells to generate calcified nodules (Fig. 8E and G). Apoptosis was also detected. Notably, the apoptotic rate of cells was again elevated in the presence of LY294002 (Fig. 8F and H). These findings indicated that the anti-apoptotic and bone-producing ability of ARC was clearly diminished following treatment with a PI3K inhibitor. Based on this, ARC may be able to treat apoptosis and osteogenic differentiation of cells under iron overload by regulating the PI3K/Akt pathway.

ARC reduces the accumulation of intracellular ROS and LPO caused by iron overload. The aforementioned findings

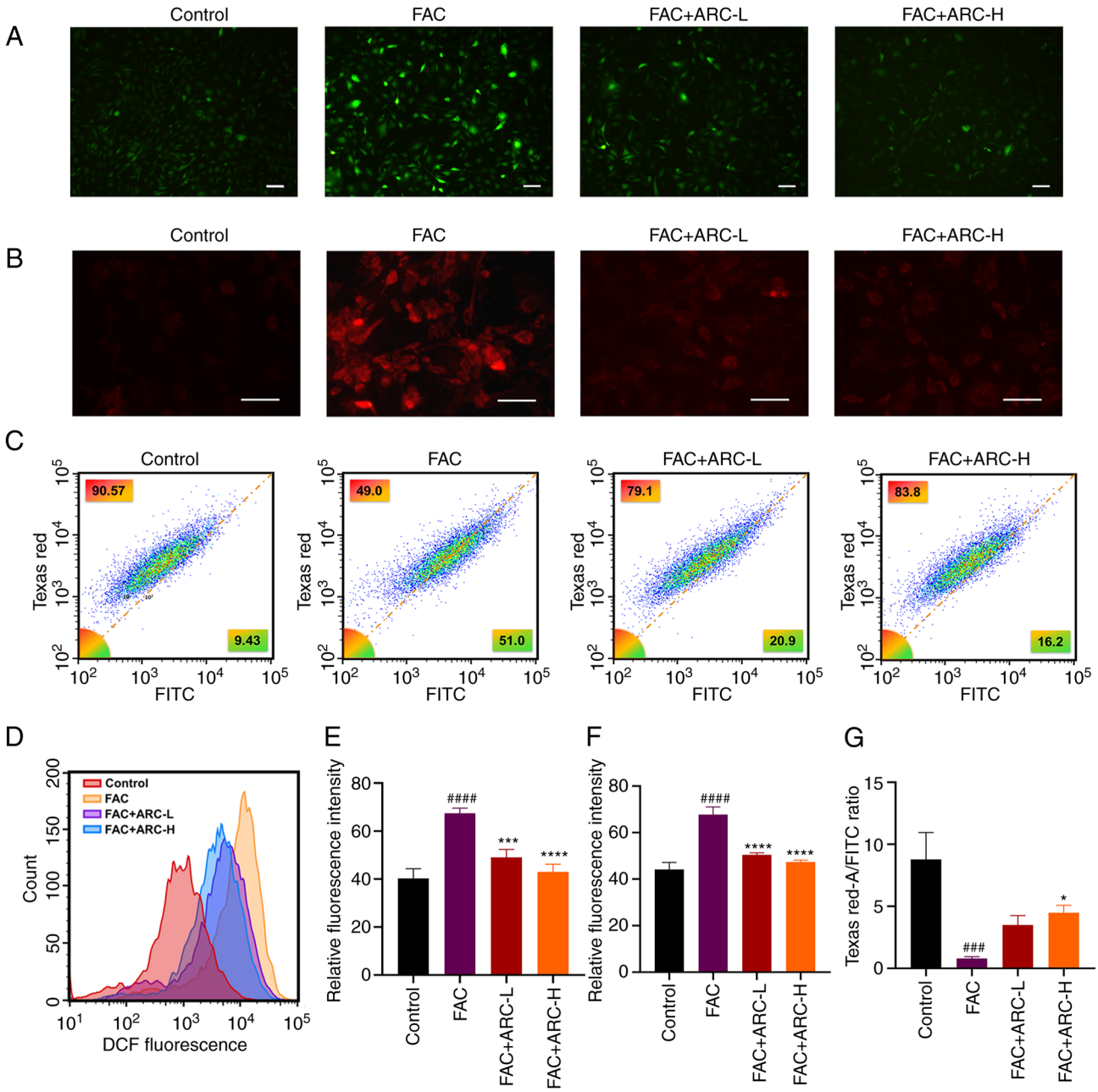

Figure 9. ARC reduces the accumulation of intracellular reactive oxygen species and LPO due to iron overload. (A) Intracellular ROS levels were detected by microscopy. Scale bar, 100 μm. (B) MC3T3-E1 cells were incubated with the MitoSOX Red Mitochondrial Superoxide Indicator and visualized by confocal microscopy. Scale bar, 50 μm. (C) Intracellular LPO levels were detected by flow cytometry after staining with the C11 BODIPY fluorescent probe. (D) Intracellular ROS levels were detected by flow cytomrtry. (E) Statistical analysis of (A). (F) Statistical analysis of staining. (G) Semi-quantification of the ratio of LPO content Texas Red-A/FITC by flow cytometry. Data are presented as the mean ± SD. ****P<0.0001, ***P<0.001 and *P<0.05 vs. Mod; $^{\#\#\#\#}$P<0.0001 and $^{\#\#\#}$P<0.001 vs. Con. ARC, arctiin; ARC-H, ARC-high; ARC-L, ARC-low; Con, control; FAC, ferric ammonium citrate; LPO, lipid peroxidation; Mod, model (500 μM FAC).

confirm the ability of ARC to alleviate iron overload-induced apoptosis through the PI3K/Akt pathway; however, iron overload is also known to increase intracellular ROS and LPO through the Fenton response, causing cytotoxic effects and further inducing apoptosis. The present study subsequently investigated the effect of ARC on oxidation in cells with iron overload. A DCFH-DA probe was used to detect the accumulation of ROS. Based on microscopic observations and flow cytometry measurements, the fluorescence intensity was significantly higher following high-dose FAC treatment, thus demonstrating the accumulation of ROS under iron overload, whereas ARC was able to reduce this in a dose-dependent manner (Fig. 9A, D and E).

Cells were also detected with the MitoSOX Red Mitochondrial Superoxide Indicator Probe in the same manner, to detect the accumulation of mtROS, and similar results to those obtained with the ROS assay were determined (Fig. 9B and F).

Intracellular LPO content under iron overload was detected by flow cytometry, and was revealed to be significantly increased by FAC compared with that in the control and ARC groups (Fig. 9C and G). These experimental results suggested

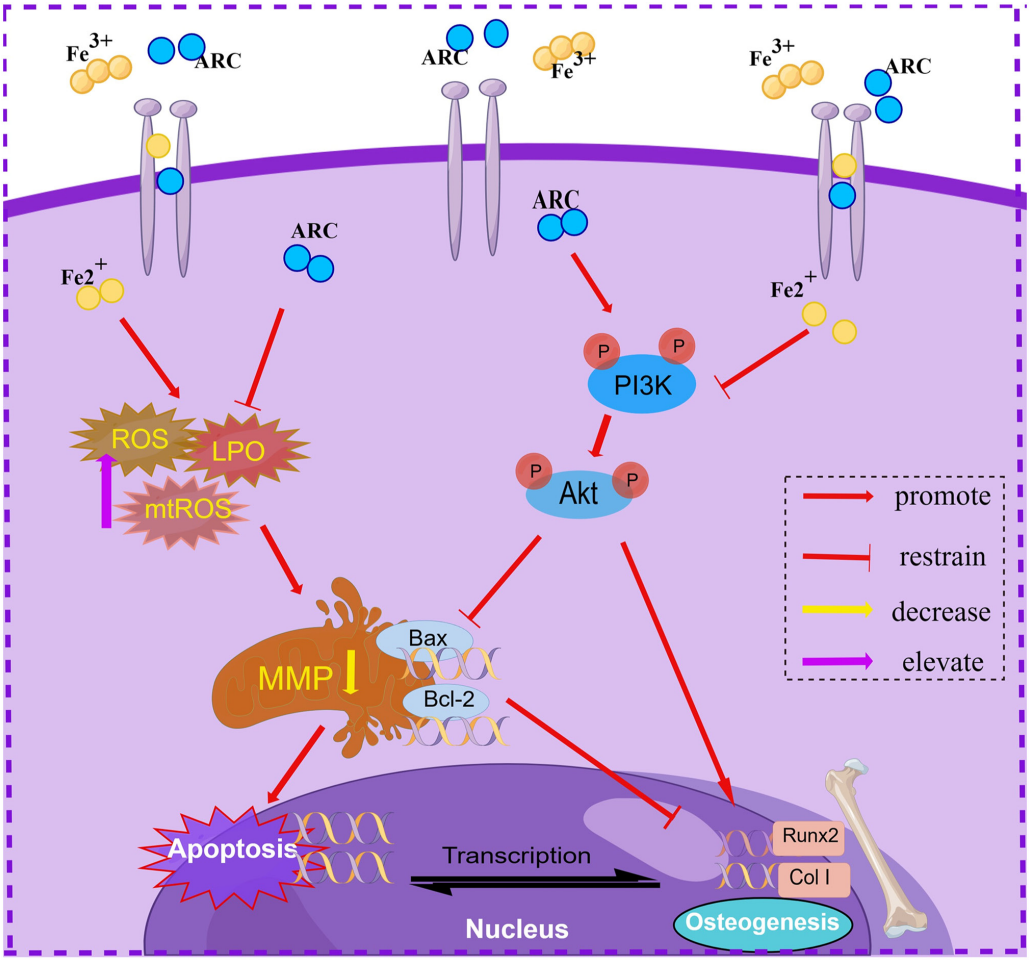

Figure 10. Diagram of the mechanism underlying the effects of ARC on iron overload-induced osteoporosis (Drawing by Figdraw, URL: https://www.figdraw.com/static/index.html#/paint_canvas?canva=350757). ARC attenuates apoptosis and promotes osteogenic differentiation of MC3T3-E1 cells by activating the PI3K/Akt pathway. It also directly attenuates the accumulation of ROS, mtROS and LPO induced by iron overload and protects cells from oxidative damage. ARC, arctiin; Col I, collagen type I; LPO, lipid peroxidation; MMP, mitochondrial membrane potential; mtROS, mitochondrial reactive oxygen species; Runx2, Runt-related transcription factor 2.

that ARC may directly reduce the intracellular levels of ROS, mtROS and LPO, and improve cell survival.

Discussion

Trace amounts of iron are essential for cell survival; however, an excess of iron promotes the generation of ROS, leading to cellular apoptosis (35). Iron overload is a pivotal factor contributing to the development of osteoporosis. It disrupts cellular redox systems, hampers bone remodeling, and impacts bone quality, microstructure and biomechanical properties, ultimately resulting in bone loss and fractures (36-38). It has previously been reported that ARC can stimulate the differentiation of MC3T3-E1 cells by modulating cell cycle proteins (27); however, to the best of our knowledge, its effects in the context of IOOP have not been reported. The present study provided the first *in vivo* evidence of the significant role of ARC in IOOP therapy using an iron overload animal model created through intraperitoneal injection of dextran iron. ARC effectively enhanced bone trabeculae and histological parameters in mice subjected to excess dextran iron. Additionally, by treating MC3T3-E1 cells with FAC an *in vitro* iron overload cell model was also established, and it was observed that ARC not only promoted ALP production and the formation of calcified nodules, but also increased the expression levels of proteins associated with osteogenic differentiation. According to these *in vivo* and *in vitro* osteogenesis-promoting phenotypic findings, the present study next proceeded to the next step of mechanistic validation. Endogenous apoptosis predominantly occurs through the mitochondrial and endoplasmic reticulum pathways (39,40). When a cell encounters internal apoptosis-inducing factors, such as DNA damage, it can activate the mitochondrial apoptosis pathway, ultimately leading to apoptosis (40). In this pathway, Bcl-2 family proteins regulate mitochondrial outer membrane permeability by modulating membrane potential (41). Upon receiving apoptotic signals, Bax relocalizes to the mitochondrial surface, reducing membrane potential and releasing apoptotic factors. The PI3K/Akt signaling pathway regulates Bax and other Bcl-2 family proteins (42,43), signifying a close interplay between mitochondrial dysfunction and the PI3K/Akt pathway. Several reports have shown that activation of the PI3K/Akt pathway promotes osteoblast proliferation and differentiation, and mitigates apoptosis and ferroptosis in MC3T3-E1 cells (17,44,45). Abdurahman *et al* (46) demonstrated in a mouse model of osteoporosis that activating the PI3K/Akt pathway enhances

osteogenesis by increasing angiogenesis. In the present study, ARC successfully restored the diminished MMP caused by excess iron and subsequently mitigated the apoptosis induced by damaged mitochondria. ARC also elevated the phosphorylation levels of PI3K and AKT. To validate these findings, LY294002, a PI3K inhibitor, was used. Western blotting showed that LY294002 again inhibited the ARC-activated PI3K/Akt pathway, reversed the increased expression levels of Col I, Runx2 and Bcl-2 proteins induced by ARC, in addition to reversing the decreased Bax expression induced by ARC. Although ARC was effective in promoting osteogenesis and inhibiting apoptosis, its efficacy was significantly diminished or disappeared following treatment with LY294002. Similarly, as determined by immunohistochemistry, p-PI3K and Runx2 were more broadly distributed in the bone trabeculae of ARC-treated mice. Therefore, these findings indicated that ARC exerts its anti-apoptotic and osteogenic effects by activating the PI3K/Akt pathway.

Oxidative stress involves multiple factors, with excess iron being a significant contributor. Iron-sulfur clusters, a primary source of intracellular ROS, primarily interact with ROS-producing enzymes, such as NADPH oxidase and xanthine oxidase, to regulate ROS levels (47). When the body experiences iron overload, these enzymes are substantially upregulated, leading to elevated levels of ROS and, ultimately, impaired cellular function and death. Furthermore, ROS generation is facilitated by iron through Fenton reactions (48). Deng *et al* (19) demonstrated that increased ROS content inhibits the activation of the PI3K/Akt signaling pathway in osteoblasts. Notably, the ROS-PI3K/AKT cascade response can lead to apoptosis (49). The present study established that ARC can regulate apoptosis and promote osteogenesis via the PI3K/Akt pathway. However, oxidative accumulation is equally capable of inducing cell death, particularly in the context of iron overload characterized by intracellular oxidative accumulation. Therefore, the present study further investigated the oxidative stress phenotype. It was observed that ARC could reduce intracellular oxidative stress induced by iron overload, thereby decreasing the production of ROS, mtROS and LPO; this may directly slow the rate of apoptosis through its antioxidant capacity.

Although the present findings suggested that ARC could promote iron excretion *in vivo* and *in vitro*, this effect was not significant. These findings indicated that ARC counteracts the adverse effects of iron overload primarily through other mechanisms, as explored in the present study. Additionally, although ARC can activate the PI3K/Akt signaling pathway and exhibit antioxidant effects, the present study did not investigate the relationship between them in-depth, thus further exploration is required. Finally, the present study was not able to conduct further evaluation of the effects of oral ARC, as well as injectable iron dextran, on other organs in the body, such as the liver and kidney. This is a limitation of the present study, as it could not be determined whether ARC has a therapeutic effect or exhibits dose toxicity on these organs.

In conclusion, the present study demonstrated that ARC has potential in mitigating IOOP *in vitro* and *in vivo*. ARC was shown to interact with the PI3K/Akt pathway, enabling anti-apoptotic properties and facilitating bone differentiation. In addition, it could directly mitigate iron overload-induced oxidative stress, shielding cells from damage (Fig. 10). These findings indicated that ARC may present a novel therapeutic approach for addressing IOOP.

Acknowledgements

Not applicable.

Funding

The present study was supported by the National Natural Science Foundation of China (grant no. 82074462), the Major Projects of Guangdong Education Department for Foundation Research and Applied Research (grant no. 2021KTSCX021), the Guangzhou Municipal Science and Technology Project (grant no. 202201020314) and the Collaborative Innovation Team Project of Guangzhou University of Chinese Medicine (grant no. 2021xk53).

Availability of data and materials

The datasets used and/or analyzed during the current study are available from the corresponding author on reasonable request.

Authors' contributions

ML conceptualized the study, participated in data analysis and wrote the original manuscript. ZP participated in data analysis and organization, wrote and reviewed the original manuscript and conceptualized the study. QH conceived the study, participated in writing and reviewing the original manuscript. ML, ZP and QH co-conceived the study, adapted the experimental ideas based on the results, wrote the manuscript, participated in data analysis and organization, and made critical revisions to the manuscript, as well as directing the animal and cell experiments. JX was responsible for animal experiments, data analysis and organization. BC was responsible for flow cytometry experiments and fluorescence experiments, data analysis and organization. FW was responsible for cell culture and fluorescence experiments, data analysis and organization. PK was responsible for cell induction experiments, in data analysis and organization. HL was responsible for cell protein imprinting experiments, data analysis and organization. JL was responsible for cell protein imprinting experiments, participating in data analysis and organization. JZ was responsible for western blotting experiments and participated in data analysis and organization. SL was responsible for animal experiments and participated in data analysis and organization. JY was responsible for animal experiments and participated in data analysis and organization. HW and CZ conceived the study, wrote, reviewed the original manuscript and was responsible for obtaining funding. All authors read and approved the final manuscript. ML and ZP confirm the authenticity of all the raw data.

Ethics approval and consent to participate

The present study was approved by the Ethics Committee of Guangzhou University of Chinese Medicine (approval no. TCMF1-2021029; May 20, 2021).

Patient consent for publication

Not applicable.

Competing interests

The authors declare that they have no competing interests.

References

1. Li Y, Bai B and Zhang Y: Bone abnormalities in young male rats with iron intervention and possible mechanisms. Chem Biol Interact 279: 21-26, 2018.
2. Manolagas SC: From estrogen-centric to aging and oxidative stress: A revised perspective of the pathogenesis of osteoporosis. Endocr Rev 31: 266-300, 2010.
3. Harrison PM, Fischbach FA, Hoy TG and Haggis GH: Ferric oxyhydroxide core of ferritin. Nature 216: 1188-1190, 1967.
4. Li GF, Pan YZ, Sirois P, Li K and Xu YJ: Iron homeostasis in osteoporosis and its clinical implications. Osteoporos Int 23: 2403-2408, 2012.
5. Tsay J, Yang Z, Ross FP, Cunningham-Rundles S, Lin H, Coleman R, Mayer-Kuckuk P, Doty SB, Grady RW, Giardina PJ, *et al*: Bone loss caused by iron overload in a murine model: Importance of oxidative stress. Blood 116: 2582-2589, 2010.
6. Chen B, Yan YL, Liu C, Bo L, Li GF, Wang H and Xu YJ: Therapeutic effect of deferoxamine on iron overload-induced inhibition of osteogenesis in a zebrafish model. Calcif Tissue Int 94: 353-360, 2014.
7. Stockwell BR, Friedmann Angeli JP, Bayir H, Bush AI, Conrad M, Dixon SJ, Fulda S, Gascón S, Hatzios SK, Kagan VE, *et al*: Ferroptosis: A regulated cell death nexus linking metabolism, redox biology, and disease. Cell 171: 273-285, 2017.
8. Nishizaki D and Iwahashi H: Baicalin inhibits the fenton reaction by enhancing electron transfer from Fe (2+) to dissolved oxygen. Am J Chin Med 43: 87-101, 2015.
9. Gao M, Yi J, Zhu J, Minikes AM, Monian P, Thompson CB and Jiang X: Role of mitochondria in ferroptosis. Mol Cell 73: 354-363.e3, 2019.
10. Feng H and Stockwell BR: Unsolved mysteries: How does lipid peroxidation cause ferroptosis? PLoS Biol 16: e2006203, 2018.
11. Hamacher-Brady A: CMLS forum reviews: Mitochondrial damage control. Cell Mol Life Sci 78: 3763-3765, 2021.
12. Yin N, Zhu L, Ding L, Yuan J, Du L, Pan M, Xue F and Xiao H: MiR-135-5p promotes osteoblast differentiation by targeting HIF1AN in MC3T3-E1 cells. Cell Mol Biol Lett 24: 51, 2019.
13. Izumiya M, Haniu M, Ueda K, Ishida H, Ma C, Ideta H, Sobajima A, Ueshiba K, Uemura T, Saito N and Haniu H: Evaluation of MC3T3-E1 cell osteogenesis in different cell culture Media. Int J Mol Sci 22: 7752, 2021.
14. Karar J and Maity A: PI3K/AKT/mTOR Pathway in Angiogenesis. Front Mol Neurosci 4: 51, 2011.
15. Yang Q, Jiang W and Hou P: Emerging role of PI3K/AKT in tumor-related epigenetic regulation. Semin Cancer Biol 59: 112-124, 2019.
16. Xu F, Na L, Li Y and Chen L: Roles of the PI3K/AKT/mTOR signalling pathways in neurodegenerative diseases and tumours. Cell Biosci 10: 54, 2020.
17. Hao J, Bei J, Li Z, Han M, Ma B, Ma P and Zhou X: Qing'e Pill inhibits osteoblast ferroptosis via ATM serine/threonine kinase (ATM) and the PI3K/AKT pathway in primary osteoporosis. Front Pharmacol 13: 902102, 2022.
18. Chen L, Liu P, Feng X and Ma C: Salidroside suppressing LPS-induced myocardial injury by inhibiting ROS-mediated PI3K/Akt/mTOR pathway in vitro and in vivo. J Cell Mol Med 21: 3178-3189, 2017.
19. Deng S, Dai G, Chen S, Nie Z, Zhou J, Fang H and Peng H: Dexamethasone induces osteoblast apoptosis through ROS-PI3K/AKT/GSK3β signaling pathway. Biomed Pharmacother 110: 602-608, 2019.
20. Cai E, Han J, Yang L, Zhang W, Zhao Y, Chen Q, Guo M and He X: Novel method of preparation and activity research on arctigenin from fructus arctii. Pharmacogn Mag 14: 87-94, 2018.
21. Gao Q, Yang M and Zuo Z: Overview of the anti-inflammatory effects, pharmacokinetic properties and clinical efficacies of arctigenin and arctiin from Arctium lappa L. Acta Pharmacol Sin 39: 787-801, 2018.
22. Liu X, Wang J, Dou P, Zhang X, Ran X, Liu L and Dou D: The ameliorative effects of arctiin and arctigenin on the oxidative injury of lung induced by Silica via TLR-4/NLRP3/TGF-β signaling pathway. Oxid Med Cell Longev 2021: 5598980, 2021.
23. Hyam SR, Lee IA, Gu W, Kim KA, Jeong JJ, Jang SE, Han MJ and Kim DH: Arctigenin ameliorates inflammation in vitro and in vivo by inhibiting the PI3K/AKT pathway and polarizing M1 macrophages to M2-like macrophages. Eur J Pharmacol 708: 21-29, 2013.
24. Lee CY, Hsin MC, Chen PN, Lin CW, Wang PH, Yang SF and Hsiao YH: Arctiin Inhibits cervical cancer cell migration and invasion through suppression of S100A4 expression via PI3K/Akt pathway. Pharmaceutics 14: 365, 2022.
25. Zhou M, Li G, Zhu L, Zhou H and Lu L: Arctiin attenuates high glucose-induced human retinal capillary endothelial cell proliferation by regulating ROCK1/PTEN/PI3K/Akt/VEGF pathway in vitro. J Cell Mol Med 24: 5695-5706, 2020.
26. Chen D, Ye Z, Wang C, Wang Q, Wang H, Kuek V, Wang Z, Qiu H, Yuan J, Kenny J, *et al*: Arctiin abrogates osteoclastogenesis and bone resorption via suppressing RANKL-induced ROS and NFATc1 activation. Pharmacol Res 159: 104944, 2020.
27. Liu Z and Wu Y: Arctiin elevates osteogenic differentiation of MC3T3-E1 cells by modulating cyclin D1. Bioengineered 13: 10866-10874, 2022.
28. Zhou B, Weng G, Huang Z, Liu T and Dai F: Arctiin prevents LPS-Induced acute lung injury via inhibition of PI3K/AKT signaling pathway in mice. Inflammation 41: 2129-2135, 2018.
29. Li G, Park JN, Park HJ, Suh JH and Choi HS: High cholesterol-induced bone loss is attenuated by arctiin via an action in osteoclasts. Nutrients 14: 4483, 2022.
30. He Q, Yang J, Pan Z, Zhang G, Chen B, Li S, Xiao J, Tan F, Wang Z, Chen P and Wang H: Biochanin A protects against iron overload associated knee osteoarthritis via regulating iron levels and NRF2/System xc-/GPX4 axis. Biomed Pharmacother 157: 113915, 2023.
31. Fernández I, Peña A, Del Teso N, Pérez V and Rodríguez-Cuesta J: Clinical biochemistry parameters in C57BL/6J mice after blood collection from the submandibular vein and retroorbital plexus. J Am Assoc Lab Anim Sci 49: 202-206, 2010.
32. Long JR, Liu PY, Lu Y, Xiong DH, Zhao LJ, Zhang YY, Elze L, Recker RR and Deng HW: Association between COL1A1 gene polymorphisms and bone size in Caucasians. Eur J Hum Genet 12: 383-388, 2004.
33. Kim WJ, Shin HL, Kim BS, Kim HJ and Ryoo HM: RUNX2-modifying enzymes: Therapeutic targets for bone diseases. Exp Mol Med 52: 1178-1184, 2020.
34. Ma Y, Abbate V and Hider RC: Iron-sensitive fluorescent probes: Monitoring intracellular iron pools. Metallomics 7: 212-222, 2015.
35. Andrews NC: Disorders of iron metabolism. N Engl J Med 341: 1986-1995, 1999.
36. Fung EB, Harmatz PR, Milet M, Coates TD, Thompson AA, Ranalli M, Mignaca R, Scher C, Giardina P, Robertson S, *et al*: Fracture prevalence and relationship to endocrinopathy in iron overloaded patients with sickle cell disease and thalassemia. Bone 43: 162-168, 2008.
37. Jomova K and Valko M: Advances in metal-induced oxidative stress and human disease. Toxicology 283: 65-87, 2011.
38. Jeney V: Clinical impact and cellular mechanisms of iron overload-associated bone loss. Front Pharmacol 8: 77, 2017.
39. Hu H, Tian M, Ding C and Yu S: The C/EBP homologous protein (CHOP) transcription factor functions in endoplasmic reticulum stress-induced apoptosis and microbial infection. Front Immunol 9: 3083, 2019.
40. Bock FJ and Tait SWG: Mitochondria as multifaceted regulators of cell death. Nat Rev Mol Cell Biol 21: 85-100, 2020.
41. Green DR: The mitochondrial pathway of apoptosis part II: The BCL-2 protein family. Cold Spring Harb Perspect Biol 14: a041046, 2022.
42. Simonyan L, Renault TT, Novais MJ, Sousa MJ, Côrte-Real M, Camougrand N, Gonzalez C and Manon S: Regulation of Bax/mitochondria interaction by AKT. FEBS Lett 590: 13-21, 2016.
43. Rahmani M, Nkwocha J, Hawkins E, Pei X, Parker RE, Kmieciak M, Leverson JD, Sampath D, Ferreira-Gonzalez A and Grant S: Cotargeting BCL-2 and PI3K Induces BAX-Dependent mitochondrial apoptosis in AML cells. Cancer Res 78: 3075-3086, 2018.

44. Gu YX, Du J, Si MS, Mo JJ, Qiao SC and Lai HC: The roles of PI3K/Akt signaling pathway in regulating MC3T3-E1 preosteoblast proliferation and differentiation on SLA and SLActive titanium surfaces. J Biomed Mater Res A 101: 748-754, 2013.
45. Ma P, Gu B, Ma J, E L, Wu X, Cao J and Liu H: Glimepiride induces proliferation and differentiation of rat osteoblasts via the PI3-kinase/Akt pathway. Metabolism 59: 359-366, 2010.
46. Abdurahman A, Li X, Li J, Liu D, Zhai L, Wang X, Zhang Y, Meng Y, Yokota H and Zhang P: Loading-driven PI3K/Akt signaling and erythropoiesis enhanced angiogenesis and osteogenesis in a postmenopausal osteoporosis mouse model. Bone 157: 116346, 2022.
47. Dixon SJ and Stockwell BR: The role of iron and reactive oxygen species in cell death. Nat Chem Biol 10: 9-17, 2014.
48. Gammella E, Recalcati S and Cairo G: Dual Role of ROS as signal and stress agents: Iron tips the balance in favor of toxic effects. Oxid Med Cell Longev 2016: 8629024, 2016.
49. Wan J, Cheng W, Xing X, He Y, Tang P, Feng Y, Liu S, Lu X and Zhong L: A SERS-Based dual-parameter monitoring nanoprobe of ROS and PI3K/Akt during Ginsenoside Rg3-induced cell apoptosis. Biosensors (Basel) 13: 212, 2023.